Performance Analysis of Eight-element MIMO Mobile Phone Antenna for Sub-6 GHz 5G Applications

Dhananjeyan Rajendran[1], Ramesh Subramaniam[1], and Rajesh Kumar Dhandapani[2]

[1]Department of Electronics and Communication Engineering
SRM Valliammai Engineering College, Chennai, Tamil Nadu, India
dhananj13@gmail.com, rameshsvk@gmail.com

[2]Department of Electronics and Communication Engineering
Vel Tech Rangarajan Dr. Sagunthala R&D Institute of Science and Technology, Chennai, Tamil Nadu, India
sdrk@gmail.com

Abstract – This paper presents an 8-port MIMO antenna array for use with 5G handsets. The proposed MIMO antenna array comprises eight U-shaped, coupled-fed slot antenna components placed symmetrically on a 0.8 mm thick FR4 substrate. Each antenna has 200 MHz bandwidth and covers 3.4-3.6 GHz. The operational frequency range includes LTE band 48 for 5G cellular applications. Using spatial and polarisation diversity, antenna components are isolated by over 15 dB. The prototype antenna is fabricated and measured, and the experimental results agree with the simulated results. The estimated Envelope Correlation Coefficient (ECC), less than 0.035 based on radiation characteristics, shows that the suggested MIMO antenna array performs well in diversity. These characteristics indicate that the proposed MIMO antenna is a viable solution for 5G smartphone applications.

Index Terms – 5G, 8-port, ECC, MIMO, sub-6 GHz.

I. INTRODUCTION

5G wireless communication will make it feasible to move large amounts of data at a high pace and engage in intelligent wireless communication. However, communication through 5G has unique challenges, such as high data rates and stringent requirements for channel capacity. The MIMO technology that supports wideband operation may be the best choice for accomplishing these goals [1, 2]. Compared to 3G and 4G smartphones, 5G devices must have MIMO that is 8×8, and must also have broadband capabilities [3, 4]. Adding more antenna components may enhance transmission rates and channel capacity. As a result, the MIMO system's overall performance would deteriorate [5–8]. Because of their restricted design, mobile phones make it hard for users to experience a greater sensation of separation from others. These technologies (MIMO), which are now accessible for commercial use, have been shown to increase system performance in terms of high data rate and channel capacity [8–14], and they are now in widespread use. Several publications have presented narrowband MIMO antenna designs for 5G smartphones. The impedance bandwidth was increased to encompass more sub-6 GHz operating bands [15–19]. The increasing distance between antenna components requires various decoupling solutions. Several different decoupling strategies have been used in the fight against isolation. MIMO isolation was enhanced by the use of spatial and polarization diversity techniques and an increase in the distance between the various antenna components [20, 21]. Improved isolation has also been achieved using hybrid resonators, EBG structures, neutralising lines, FSC, and inverted-I ground slot technologies [22, 23]. According to research, additional decoupling techniques have the potential to improve isolation, yet they also increase the complexity of production and take up valuable real estate on the system board. The significance of this work may be summed up as follows. This article proposes an eight-input MIMO antenna for 3.4-3.6 GHz.

We have raised the isolation between antenna components by more than 15 dB, improving radiation efficiency by 68-76% in our target band of operation. This was accomplished without the assistance of decoupling structures. The MIMO antenna with an ECC of 0.035 and a channel capacity of 38.789 bps/Hz is the one that is suggested. All design particulars of the proposed antenna have been validated using HFSS electromagnetic simulator.

The originality of the work may be summed up as follows:

(1) Better than 15 dB of mutual coupling may be achieved between the antenna elements without specialised processes or methods.
(2) A reduction in the mutual coupling leads to higher MIMO performance in terms of overall

Submitted On: December 16, 2023
Accepted On: June 18, 2024
https://doi.org/10.13052/2024.ACES.J.390405

radiation efficiency (68-76%) and Envelope Correlation Coefficient (ECC). This is because a decrease in the mutual coupling leads to fewer interactions between the antennas (ECC$<$0.035).

(3) The total diameter of the individual antenna is very small which leads to the system PCB board being able to accommodate up to eight antennas.

(4) Despite its small size, the suggested antenna can cover a reasonable range of the electromagnetic spectrum, from 3.4 to 3.6 GHz.

II. ANTENNA DESIGN AND ANALYSIS

The geometry and general construction of the proposed 8-port MIMO antenna array are depicted in detail in Figs. 1 (a) and (b), respectively. As shown in Fig. 1 (a), each antenna component is printed on an FR4 substrate with the following dimensions: 150 millimetres long, 80 millimetres wide, and 0.8 millimetres thick. These measurements make the substrate suitable for smartphones with screens measuring up to 5.7 inches in diagonal length.

Antenna elements 6 to 8 occupy the substrate's left-side edges, and antenna elements 2 to 4 occupy the right-side edges of the substrate. Figure 1 provides a comprehensive illustration of the particulars of antenna 1's construction and its dimensions. The slot radiator, also known as antenna 1, is made up of three different rectangular slots connected to one another to produce a U-shaped open-ended slot. The initial step of the technique involves cutting the ground plane along its top short edge to create a rectangular slot with dimensions 9.5×6.5 mm. Figure 1 (b) illustrates the process of carving two rectangular slots, each of which has the following dimensions: 15×7 mm and 5.5×0.2 mm, respectively. A minute slit open on all four sides and shaped like a square is cut into the surface of the ground plane that is closest to the top of the structure. All of the carved slots mentioned earlier are combined, and then the combined slot is tuned to resonate at 3.4-3.6 GHz, creating an open-ended T-shaped slot.

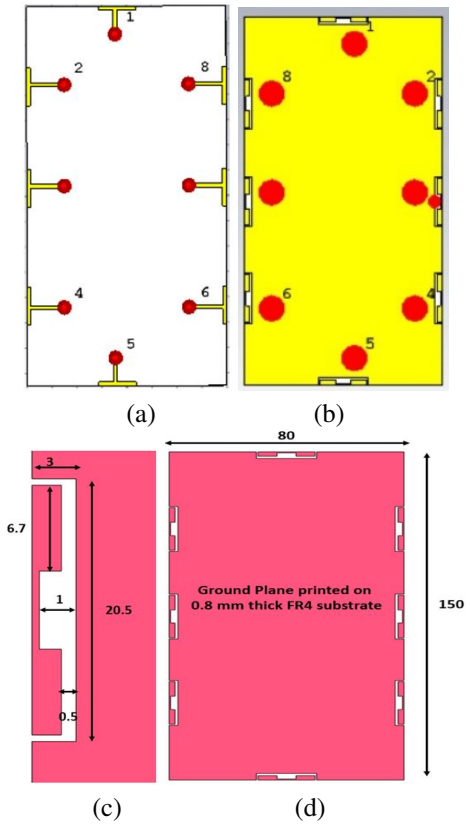

Fig. 1. *Continued*

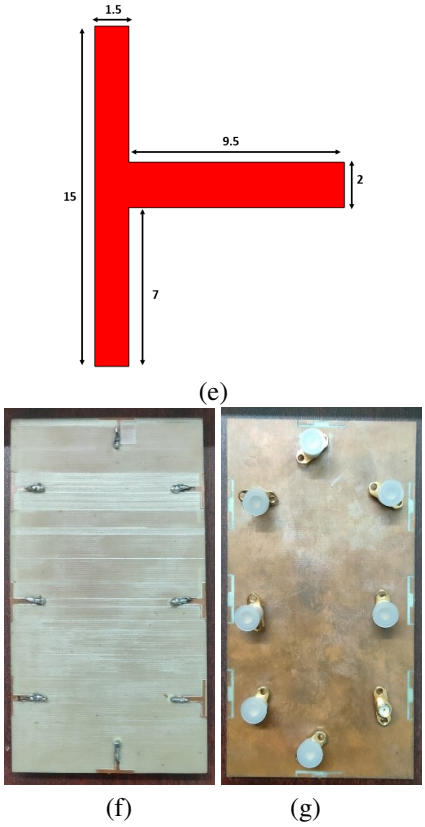

Fig. 1. (a,b) Front and back view of the simulated antenna, dimensions of (c) slot in the ground plane, (d) ground plane, (e) feeding stub, and (f,g) front and back view of the prototype of the proposed antenna.

III. RESULTS AND DISCUSSION

Figures 2 (a-e) depict the manufacturing process as well as the testing of the 8-port MIMO antenna array prototype that has been proposed. To carry out the measurements, 50-ohm SMA female connectors are attached to the feeding strips associated with the antenna components. An antenna's S-parameters, isolation, and

radiation pattern can be evaluated by first exciting the antenna to be tested and then connecting all of the antenna's elements to matched loads of 50 ohms. The reflection and transmission coefficients, both simulated and measured, for the 8-port antenna array under consideration are illustrated in Figs. 2 (a) and (d) and Figs. 2 (b) and (e), respectively.

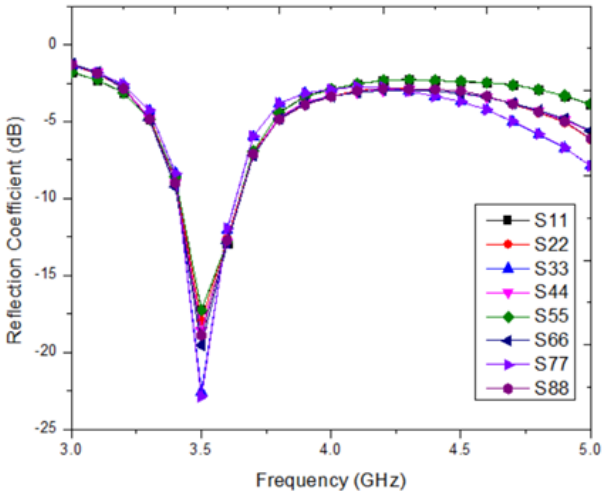

(a)

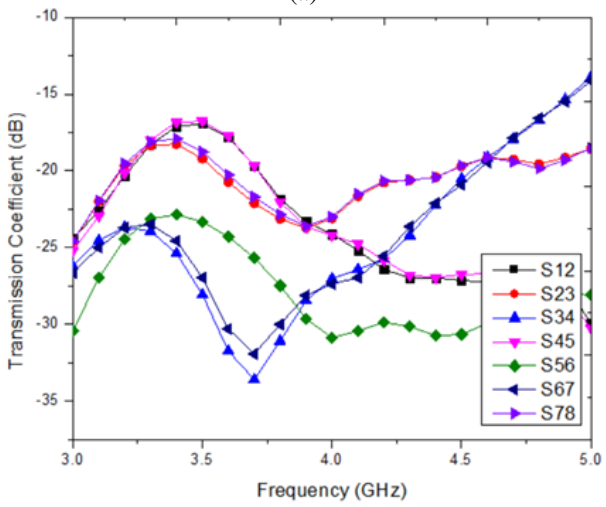

(b)

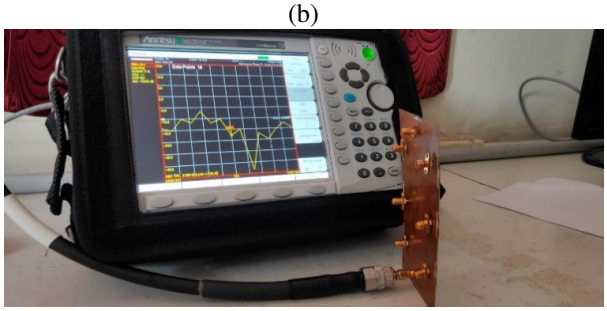

(c)

Fig. 2. *Continued*

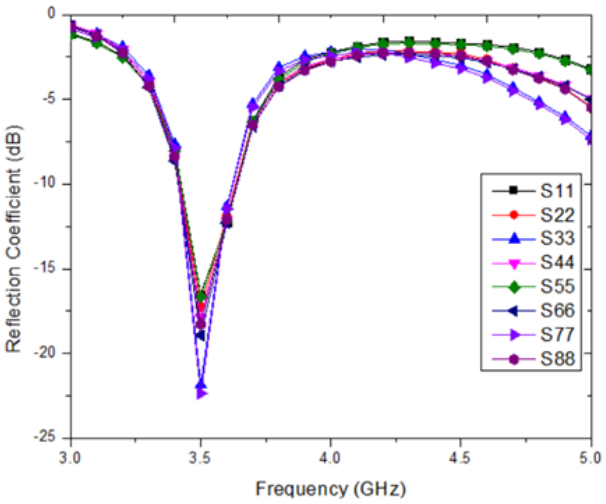

(d)

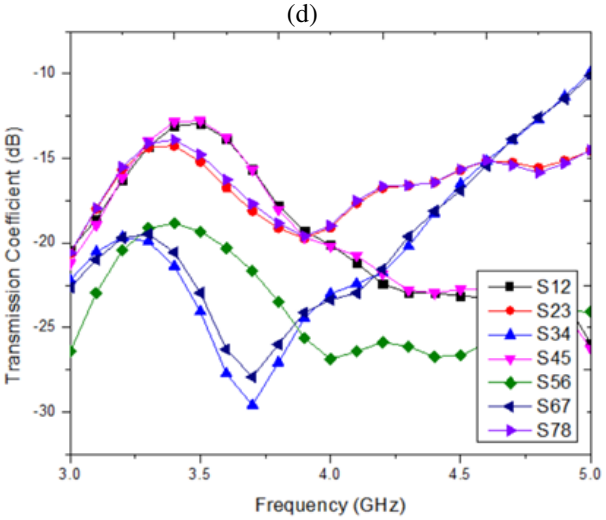

(e)

Fig. 2. (a,b) Simulated scattering parameters, (c) measurement setup, and (d,e) measured scattering parameters.

As a result of the fact that all antenna components are designed to be vertically symmetrical with respect to the centre line of the PCB, the S-parameters of antenna 2 to antenna 4 will typically be the same as those of antenna 6 to antenna 8. As can be seen in Figs. 2 (a) and (d), the simulated and measured reflection coefficients of antenna 1-8 in the 3.4-3.6 GHz operating bands, which correspond to the frequencies used for 5G applications, are less than -10 dB (2:1 Voltage Standing Wave Ratio). As shown in Figs. 2 (b) and (e), the transmission coefficients of neighbouring pairs are more than -15 dB if there is adequate distance between each antenna. In the work that is being suggested, no decoupling technique has been used to increase the isolation between the components.

This is because the open end has the lowest current, and the closed end has the highest current. Figures 3 (a) and (b) show surface currents at 3.5 GHz for antenna 1 and 2, respectively. This indicates that the T-shaped slot's fundamental mode is quarter wavelength mode. Open-ended slots of varying lengths generate the resonances at 3.5 GHz.

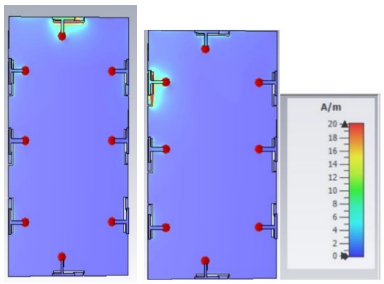

(a) (b)

Fig. 3. Surface current distribution at 3.5 GHz: (a) antenna 1 and (b) antenna 2.

To provide a design insight of the proposed antenna, a parametric study has been carried out (with a limited number of points during simulation) as shown in Figs. 4 (a) and (b), respectively. As shown in Fig. 4 (a), when altering the slot length L1 from 17.5 mm to 20.5 mm, centre frequency has been shifted with a poor reflection coefficient. It is observed that the higher the value of slot length, the better the impedance matching of the antenna. A similar response has been observed when changing feed length L1 from 12 to 15 mm as illustrated in Fig. 4 (b). For brevity, other performance metrics concerning other antenna design parameters have not been shown here.

Figures 5 (a) and (b) depict the measured radiation patterns of antennas 1 and 2, respectively. Each antenna has an omnidirectional radiation pattern (no deep null is visible throughout the pattern). The radiation patterns exhibit mutual reinforcement and symmetry, indicating that the proposed antenna possess diverse patterns.

Figure 6 illustrates the radiation efficiency of antennas 1-8, which varies from 68 to 76% over the necessary working band of the device. The large gain in overall efficiency is primarily attributable to the greater isolation between antenna components.

$$ECC = \left| \frac{\oiint A_{ij}(\theta,\varphi)\sin\theta d\theta d\varphi}{\oiint A_{ii}(\theta,\varphi)\sin\theta d\theta d\varphi \cdot \oiint A_{jj}(\theta,\varphi)\sin\theta d\theta d\varphi} \right|^2, \quad (1)$$

where:

$$A_{ij} = E_{\theta,i}(\theta,\varphi)\cdot E^*_{\theta,j}(\theta,\varphi) + E_{\varphi,i}(\theta,\varphi)\cdot E^*_{\varphi,j}(\theta,\varphi). \quad (2)$$

The observed ECCs of all array pairs are less than 0.5, as demonstrated in Fig. 7 (a), well within acceptable ranges. An 8-port antenna array that can achieve a high diversity gain with a low ECC value is a significant achievement.

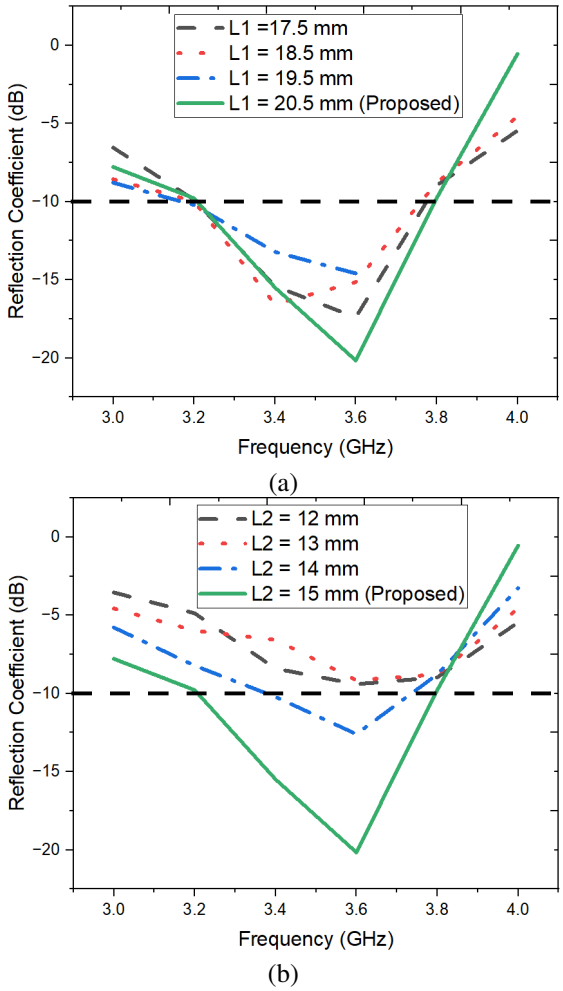

Fig. 4. Parametric analysis when altering: (a) L1 and (b) L2.

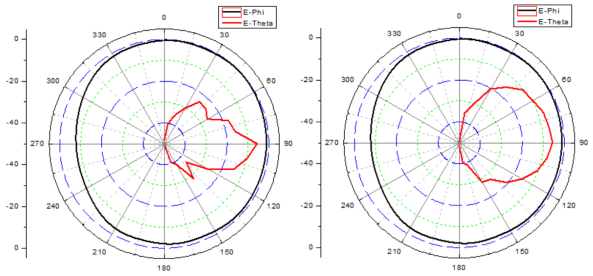

(a) (b)

Fig. 5. Two-dimensional measured radiation pattern of the (a) antenna 1 and (b) antenna 2.

To confirm the efficiency of the antenna's bandwidth, the Total Active Reflection Coefficient (TARC)

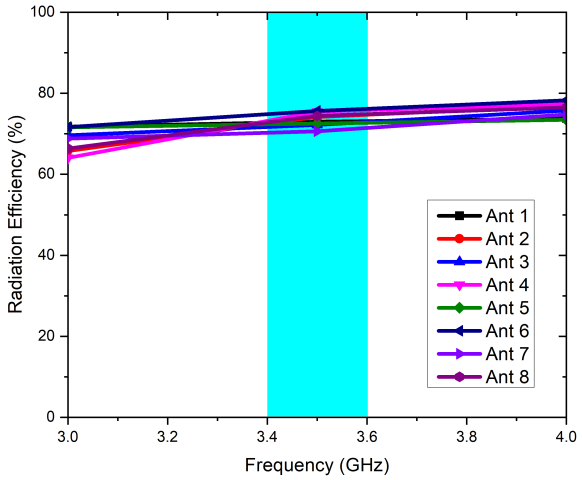

Fig. 6. Radiation efficiency of antenna (Ant) 1-8.

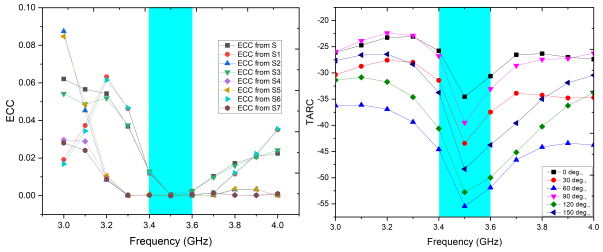

(a) (b)

Fig. 7. (a) ECC and (b) TARC of the proposed antenna.

has been graphed by adjusting the phase angle of port 1 [20], as depicted in Fig. 7 (b). All antenna elements can cover the desired frequency spectrum:

$$C = E\left(\log_2\left(\det\left(I_M + \frac{SNR_{20}dB}{M}H\left(H^T\right)\right)\right)\right). \quad (3)$$

Using equation (3), the channel capacity of the proposed antenna has been calculated.

A. Effects of handgrip

The hand phantom's impact on the antenna's performance will be discussed in this part. The Single-Handed Mechanism (SHM) and the Two-Handed Mechanism (THM) are two common types of implementations shown in Figs. 9 and 10, respectively. However, the effects of the user's head hits are not discussed, and multi-port MIMO operating at frequencies sub-6 GHz may be used for the data mode. Antennas 2, 3, and 4 are all attached to the fingers in SHM by a direct connection. This arrangement considerably influences the reflection coefficients of antennas 2, 3, and 4, as shown in Fig. 9 (a). In this scenario, antenna 8 also shows unfavourable impedance matching. Other antennas show very slight variations in their resonant modes due to the significant distance separating them from the fingers.

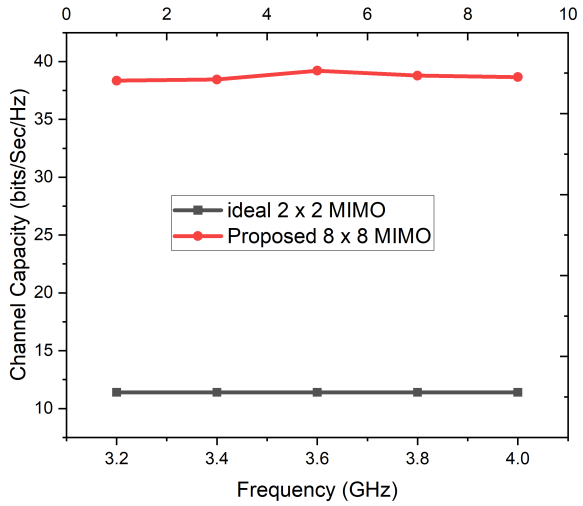

Fig. 8. Channel capacity of the proposed antenna.

Nevertheless, as shown in Fig. 9 (b), a strong barrier to outside interference (>10 dB) is achievable across the whole usable frequency range.

Due to the absorption of radiation by the hand tissue, the efficiency of antennas 2, 3, and 4 has decreased to below 40%. Because antennas 2, 3, and 4 are positioned close to the fingers, the palm's ability to absorb power has also reduced their efficiency to somewhere about 30%. Other antennas have achieved overall efficiencies of higher than 45%. This is because they are placed further away from the hand. As may be observed in

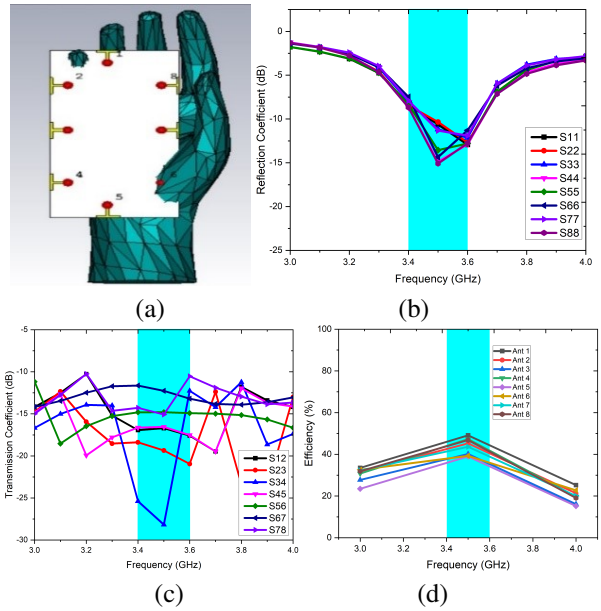

(a) (b) (c) (d)

Fig. 9. (a) Antenna with single hand phantom and (b-d) performance of the antenna with single hand phantom.

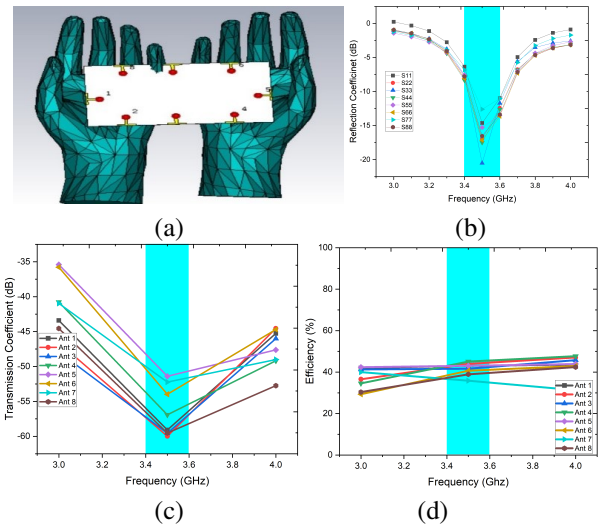

Fig. 10. (a) Antenna with two hand phantom and (b-d) performance of the antenna with two hand phantom.

Fig. 9 (a), the reflection coefficients of antennas 6, 7, and 8 suffer a small degradation when thumbs are used to cover them. Because the other antenna elements are situated near the hand phantom, their resonance properties are the same. As can be observed in Fig. 9 (c), the isolation is more than 10 dB over the whole operational spectrum. As shown in Fig. 9 (d), the overall efficiency of all antenna elements is less than 50% due to the presence of a hand phantom.

However, the overall efficiency of other antennas (located above the little fingers) is greater than 48%. As a consequence of this, it indicates that the 8-port antenna that was recommended has significant performance in contexts that operate in real-time. The effect of the head phantom model has also been investigated to validate the antenna's performance, and corresponding SAR values have been listed in Table 1. It proves the antenna exhibits maximum SAR below 1 W/kg for both 1 g and 10 g of tissue.

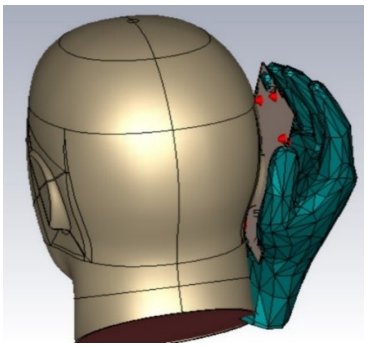

Fig. 11. Antenna with head phantom.

Table 1: SAR values of antenna 1 and antenna 2

SAR (W/kg)	Antenna 1	Antenna 2
1 g tissue	0.985	0.97458
10 g tissue	0.654	0.6845

Table 2: Performance comparison of the proposed antenna

Ref No	S (mm)	BW (MHz)	I (dB)	E (%)	ECC	N	CC (bps /Hz)
3	17.4×6	200	19.6	65-70	<0.0125	8	34
5	7.5×6	300	15	40	<0.15	8	35
8	21×3	200	17.5	62	<0.05	8	40.8
9	30×30	600	13	75	<0.01	8	NA
15	9.6×10	200	11.2	51-59	<0.1	8	36.9
17	6.6×6	300	15.1	60-80	<0.21	8	NA
This work	**13×5.2**	**200**	**15**	**68-76**	**<0.035**	**8**	**38.78**

Key: S=size of the antenna, BW=bandwidth, I=isolation, E=efficiency, N=no. of elements, CC=channel capacity.

Table 1 compares the performance of the recommended MIMO antenna array and the performance of other present MIMO antenna arrays for 5G mobile devices. In addition to its many benefits, the recommended method offers significant radiation and MIMO performance, superb isolation (more than 15 dB), and a low ECC of 0.035.

The proposed antenna, measuring 13×5.2 mm, delivers a bandwidth of 200 MHz and 15 dB isolation. With an efficiency ranging from 68 to 76%, it surpasses most counterparts. Its error correction coding of <0.035 ensures robust performance. Offering 8 ports and a channel capacity of 38.78 bps/Hz, it excels in efficiency and error correction. These attributes position it as a competitive choice, balancing size, performance, and capability effectively for the intended application.

IV. CONCLUSION

An 8-port MIMO antenna system for a 5G mobile phone operating at 3.5 GHz has been tested and successful. Neighbouring antenna components have high isolation (>15 dB). Consequently, the radiation efficiency might be increased to 68-76% throughout the operational spectrum, bringing the ECC down to less than 0.01. When the signal-to-noise ratio is 20 dB, the expected peak channel capacity in an eight-element MIMO configuration is 38.789 bps/Hz, over 11 times more than the capacity of a Single Input Single Output system. As a result, the 8-port antenna described in this paper may be a great option for the hardware and software of future generations of mobile phones.

ACKNOWLEDGMENT

The authors would like to express their gratitude to DST-FIST for providing the supporting facilities that are available at the Department of Electronics and Communication Engineering at SRM Valliammai Engineering College in Chennai, Tamil Nadu, India.

REFERENCES

[1] J. G. Andrews, S. Buzzi, W. Choi, S. V. Hanly, A. Lozano, A. C. K. Soong, and J. C. Zhang, "What will 5G be?," *IEEE Journal on Selected Areas in Communications*, vol. 32, no. 6, pp. 1065-1082, 2014.

[2] M. A. Jensen and J. W. Wallace, "A review of antennas and propagation for MIMO wireless communications," *IEEE Transactions on Antennas and Propagation*, vol. 52, no. 11, pp. 2810-2824, 2004.

[3] A. Zhao and Z. Ren, "Size reduction of self-isolated MIMO antenna system for 5G mobile phone applications," *IEEE Antennas and Wireless Propagation Letters*, vol. 18, no. 1, pp. 152-156, 2019.

[4] Jiagang He, Shichao Zhu, Jie Yu, Hao Li, and Gaosheng Li, "Wideband decoupled 8-element MIMO mobile phone antenna for sub-6 GHz 5G NR bands," *ACES Journal*, vol. 37, no. 12, pp. 1208-1215, 2022.

[5] W. Jiang, B. Liu, Y. Cui, and W. Hu, "High-isolation eight-element MIMO array for 5G smartphone applications," *IEEE Access*, vol. 7, pp. 34104-34112, 2019.

[6] M.-Y. Li, Y.-L. Ban, Z.-Q. Xu, J. Guo, and Z.-F. Yu, "Tri-polarized 12-antenna MIMO array for future 5G smartphone applications," *IEEE Access*, vol. 6, pp. 6160-6170, 2018.

[7] X. Zhao, S. P. Yeo, and L. C. Ong, "Decoupling of inverted-F antennas with high-order modes of ground plane for 5G mobile MIMO platform," *IEEE Transactions on Antennas and Propagation*, vol. 66, no. 9, pp. 4485-4495, 2018.

[8] Y. Li, C.-Y.-D. Sim, Y. Luo, and G. Yang, "High-isolation 3.5 GHz eight-antenna MIMO array using balanced open-slot antenna element for 5G smartphones," *IEEE Transactions on Antennas and Propagation*, vol. 67, no. 6, pp. 3820-3830, 2019.

[9] S. Syedakbar, S. Ramesh, and V. Ramya "Orthogonally integrated hybrid antenna for intelligent transportation systems," *Applied Computational Electromagnetics Society (ACES) Journal*, vol. 36, no. 05, pp. 519-524, May 2021.

[10] N. O. Parchin, Y. I. A. Al-Yasir, A. H. Ali, I. Elfergani, J. M. Noras, J. Rodriguez, and R. A. Abd-Alhameed," Eight-element dual-polarized MIMO slot antenna system for 5G smartphone applications," *IEEE Access*, vol. 7, pp. 15612-15622, 2019.

[11] Z. Ren, A. Zhao, and S. Wu, "MIMO antenna with compact decoupled antenna pairs for 5G mobile terminals," *IEEE Antennas and Wireless Propagation Letters*, vol. 18, no. 7, pp. 1367-1371, 2019.

[12] L. Sun, H. Feng, Y. Li, and Z. Zhang, "Compact 5G MIMO mobile phone antennas with tightly arranged orthogonal-mode pairs," *IEEE Transactions on Antennas and Propagation*, vol. 66, no. 11, pp. 6364-6369, Nov. 2018.

[13] Y. Liu, A. Ren, H. Liu, H. Wang, and C.-Y.-D. Sim, "Eight-port MIMO array using characteristic mode theory for 5G smartphone applications," *IEEE Access*, vol. 7, pp. 45679-45692, 2019.

[14] N. Kumaran, S. Ramesh, and S. Chitra, "Bandwidth and frequency agile MIMO antenna for cognitive vehicular communications," *International Journal of Communication Systems*, vol. 36, no. 14, pp. 1-18, Sep. 2023.

[15] Y. Li, C.-Y.-D. Sim, Y. Luo, and G. Yang, "Multiband 10-antenna array for sub-6 GHz MIMO applications in 5-G smartphones," *IEEE Access*, vol. 6, pp. 28041-28053, 2018.

[16] J. Li, X. Zhang, Z. Wang, X. Chen, J. Chen, Y. Li, and A. Zhang," Dualband eight-antenna array design for MIMO applications in 5G mobile terminals," *IEEE Access*, vol. 7, pp. 71636-71644, 2019.

[17] Y.-L. Ban, C. Li, C.-Y.-D. Sim, G. Wu, and K.-L. Wong, "4G/5G multiple antennas for future multi-mode smartphone applications," *IEEE Access*, vol. 4, pp. 2981-2988, 2016.

[18] A. Zhao and Z. Ren, "Wideband MIMO antenna systems based on coupled-loop antenna for 5G N77/N78/N79 applications in mobile terminals," *IEEE Access*, vol. 7, pp. 93761-93771, 2019.

[19] Q. Chen, H. Lin, J. Wang, L. Ge, Y. Li, T. Pei, and C.-Y.-D. Sim," Single ring slot-based antennas for metal-rimmed 4G/5G smartphones," *IEEE Transactions on Antennas and Propagation*, vol. 67, no. 3, pp. 1476-1487, 2019.

[20] X. Zhang, Y. Li, W. Wang, and W. Shen, "Ultra-wideband 8-Port MIMO antenna array for 5G metal-frame smartphones," *IEEE Access*, vol. 7, pp. 72273-72282, 2019.

[21] K. Kayalvizhi and S. Ramesh, "A novel MIMO antenna with switchable UWB/5G modes for vehicular terminals," *Microwave and Optical Technology Letters*, vol. 65, no. 9, pp. 2640-2645, Sep. 2023.

[22] Yonghao Wang, Xin Wang, Junlin Wang, and Rui Shao," Dual-band highly isolated eight-element MIMO antenna for 5G mobile phone," *ACES Journal*, vol. 37, no. 5, pp. 588-596, 2022.

[23] J. Deng, J. Li, L. Zhao, and L. Guo, "A dual-band inverted-F MIMO antenna with enhanced isolation for WLAN applications," *IEEE Antennas and Wireless Propagation Letters*, vol. 16, pp. 2270-2273, 2017.

Dhananjeyan Rajendran is an Assistant Professor with 14 years' teaching experience at SRM Valliammai Engineering College, Chennai. His research interests include MIMO antenna design. He is a lifetime member of IETE, ISTE.

Ramesh Subramaniam is a professor with 21 years' teaching experience at SRM Valliammai Engineering College in Chennai. He is a senior member of the IEEE Antennas & Propagation Society (S'10-M'17-SM'18). His research interests include antenna design.

Rajesh Kumar Dhandapani is an Assistant Professor with 11 years' teaching experience at Vel Tech Rangarajan Dr. Sagunthala R&D Institute of Science and Technology, Chennai. His research interests include mobile phone antenna design and RF system design.